COBEM 2021 26th International Congress of Mechanical Engineering
November 22-26, 2021, Virtual Congress, Brazil
ABCM Associação Brasileira de Engenharia e Ciências Mecânicas

COB-2021-0601
OPTIMAL CONTROL BASED ON THE REDUCED-ORDER MODEL OF A PARALLEL MANIPULATOR WITH FLEXIBLE LINKS

Fernanda Thaís Colombo
Maíra Martins da Silva
University of São Paulo, São Carlos School of Engineering, Department of Mechanical Engineering, Trabalhador São-Carlense, 400, zip code 13566-590, São Carlos, Brazil.
fernanda.colombo@usp.br, mairams@sc.usp.br

Abstract. *Flexible robotics with lightweight structures may have improved dynamic performance with high operating speeds and lower energy consumption. To address the unwanted vibration, control strategies based on their model can be crucial. In this paper, the dynamic of a parallel and planar 3RRR manipulator with flexible links is modeled in a multibody dynamics (MBD) environment using the Finite Element (FE) method. Due to the high degrees of freedom of the FE model, Model Order Reduction methods have been investigated. We validated the reduced-order model obtained by comparing its frequency domain properties with the original full-order one. The design of control strategies for parallel manipulators is challenging since their dynamics depend on the end-effector's pose and yield nonlinearities. So, we evaluated the theoretical dynamic performance in the time domain of optimal controllers based on the reduced-order model. To illustrate the controller capabilities of tracking the trajectory while also decreasing the vibration, we applied reference signals in the Cartesian space with different accelerations to this flexible manipulator. These numerical results, regarding the reduction of the FE model and the controller performance, can demonstrate the importance of model-based control strategies for lightweight manipulators with flexible links.*

Keywords: *model-based control, multibody dynamic system, model order reduction, flexible manipulators, parallel kinematic manipulators.*

1. INTRODUCTION

Parallel manipulators (PMs) have higher positioning accuracy and payload to weight ratio than their serial counterparts, but they can present singularities in the workspace (Fontes and da Silva, 2016). The design of control strategies for parallel manipulators is also challenging since their configuration depends on the end-effector's pose (Paccot *et al.*, 2009; de Carvalho Fontes *et al.*, 2018), and they have nonlinear dynamics, especially at high speeds.

Flexible robotic systems with lightweight structures may have improved dynamic performance with high operating speeds and lower energy consumption. This improvement can be achieved by reducing the inertia of their moving components (Zhang *et al.*, 2015). However, due to this modification, these flexible systems may be subjected to unwanted vibration. In this case, model-based control strategies should be employed to guaranteeing performance and stability.

Joint space model-based control strategies require the calculation of the inverse kinematic model (IKM) (Paccot *et al.*, 2006), which relates the task space to the joint space. This is not a trivial task for flexible PMs. On the other hand, Cartesian control strategies require the measurement of the end-effector pose that can be implemented by vision-based techniques and image processing algorithms (Colombo *et al.*, 2019). The latter approach requires the use of a high-speed camera and efficient image processing algorithms due to the presence of unwanted vibration, which might be a costly alternative. Strategies for estimating the Cartesian space could be highly advantageous. This can also be accomplished by deriving reliable kinematic and dynamic models. Some strategies for deriving accurate and computationally efficient dynamic models for PMs are presented in (Yang *et al.*, 2018; Zhang *et al.*, 2021). One alternative to cope with real-time requirements is to use model simplification techniques, such as model reduction techniques, as demonstrated for serial and hybrid manipulators by da Silva *et al.* (2010); Wang *et al.* (2009); Zhang *et al.* (2015); Cammarata and Maddío (2021); Yavuz and İlman (2020).

In this paper, the dynamic of a parallel and planar 3RRR manipulator with flexible links, illustrated in Fig. 1, is modeled in a multibody dynamics (MBD) environment using the Finite Element (FE) method. Another advantage of computing an MBD model is that it allows the direct measurement of the robot's end-effector position in the Cartesian space, a complex task for PMs. However, FE models of robotic systems may have tens of thousands of degrees of freedom, used to describe the deformation of the several nodes created by the mesh. Since these large-scale models are unsuitable for the control design, we applied Model Order Reduction methods to the model under study. We validated the reduced-order model obtained by comparing its frequency domain properties with the original full-order one.

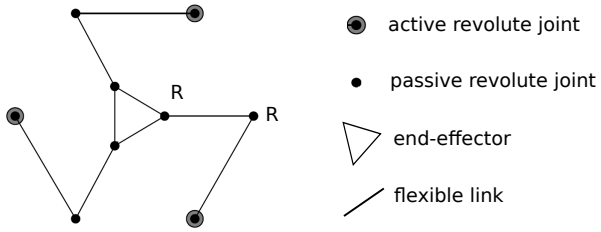

Figure 1. A illustration of the 3RRR with flexible links: a planar PM with 3 kinematic chains

To verify the applicability of the derived reduced models, we evaluate the theoretical dynamic performance in the time domain of optimal controllers designed based on the reduced-order model. To illustrate the controller capabilities of tracking the trajectory while also decreasing the vibration, we apply reference signals in the Cartesian space with different accelerations to this flexible manipulator. Performance indices in the time domain, such as the root mean squared error and energy consumption, are also analyzed.

This work is organized as follows. Section 2 briefly revises the theoretical aspect of the exploited techniques: Finite Element method, Model Reduction techniques, and the LQR Optimal Control approach. Section 3 described the model and prototype. Results are presented and discussed in Section 4, while conclusions are drawn in Section 5.

2. METHODS

The main methods used to derive a low-order dynamic model of a robotic manipulator suitable for control design are discussed in this section.

2.1 Finite Element Analysis

Many physical problems, such as the boundary value problem, can be described using partial differential equations in space and time domains. Since most practical ones don't have an exact solution, the finite element method can be used to find a numerical approximation of the solution by replacing the original complex problem with a finite number of simpler ones. In a structural mechanics problem, a system with complex geometry can be subdivided into several small pieces. These elements are interconnected to each other by nodes located on the boundaries. Physical principles, like the variational method or equilibrium conditions, are applied during the analysis of each element to derive expressions for the elementary characteristics, such as the mass and stiffness matrices and load vector. Assuming that the displacement field within an element is a piecewise continuous function, the displacement of the several nodes of the structure can be approximated by an interpolation function, usually a polynomial. This process transforms the original partial differential equation into a system of differential equations where the nodal displacements are the unknown variables. The overall dynamic equilibrium of the structure is derived by appropriately assembling the elementary matrices and vectors, as

$$\mathbf{M}\,\ddot{\mathbf{q}} + \mathbf{K}\,\mathbf{q} = \mathbf{f}, \tag{1}$$

where $\mathbf{M}$ and $\mathbf{K}$ are the assembled mass and stiffness matrices, $\mathbf{q}$ and $\mathbf{f}$ are the vectors of the nodal displacements and loads, respectively. For a structure with 3-dimensional elements and n nodes, the size of the nodal vectors is $3n$, considering that each node has three translational degrees of freedom ($\mathbf{q}_i = (x_i, y_i, z_i)^T$).

The finite element method should also satisfy the boundary conditions specified for the problem that may prescribe the motion of a set of nodes or apply force and moments to a surface. In some applications, these boundary conditions can be expressed by equality constraints (Géradin and Rixen, 2015):

$$\mathbf{H}\,\mathbf{q} = \mathbf{h}, \tag{2}$$

where $\mathbf{H}$ is a rectangular matrix and $\mathbf{h}$ is a constant vector. The finite element packages are usually responsible for the formulation of the element characteristics and the assembly of the set of equations, which may need to be scaled to guarantee that the magnitude of the displacement and load vectors are not significantly different. Additionally, they incorporate the boundary conditions into the dynamics equation of the system, as seen by

$$\begin{aligned} &\mathbf{M}\,\ddot{\mathbf{q}} + \mathbf{K}\,\mathbf{q} = \mathbf{f} \text{ subject to } \mathbf{H}\,\mathbf{q} = \mathbf{h} \\ &\quad \Leftrightarrow \bar{\mathbf{M}}\,\ddot{\bar{\mathbf{q}}} + \bar{\mathbf{K}}\,\bar{\mathbf{q}} = \bar{\mathbf{f}}, \end{aligned} \tag{3}$$

where $\bar{\mathbf{M}}$ and $\bar{\mathbf{K}}$ are the modified mass and stiffness matrices, respectively, and $\bar{\mathbf{f}}$ is the modified vector of nodal loads such that the boundary conditions are satisfied. The vector $\bar{\mathbf{q}} \in \mathbb{R}^{\bar{n}}$ consists of the remaining nodal displacements that

are not restricted by the constraints imposed on the system, with $\bar{n} \leq 3n$. To obtain the relation between the inputs and outputs of the system to be used in control design, the input $\mathbf{u} \in \mathbb{R}^{n_u}$ and output $\mathbf{y} \in \mathbb{R}^{n_y}$ vectors are defined as

$$\begin{aligned} \bar{\mathbf{f}} &= \mathbf{b}_f \, \mathbf{u}, \\ \mathbf{y} &= \mathbf{c}_y \, \bar{\mathbf{q}}, \end{aligned} \tag{4}$$

where n_u and n_y are the number of inputs and outputs, respectively. The Boolean matrices $\mathbf{b}_f \in \mathbb{R}^{\bar{n} \times n_u}$ and $\mathbf{c}_y \in \mathbb{R}^{n_y \times \bar{n}}$ are used to specify which degrees of freedom of the nodal vector $\bar{\mathbf{q}}$ are being actuated or measured.

The transient response of this system describes how its displacement vector change over time due to the forces applied $\bar{\mathbf{f}}(t)$ and initial conditions defined as

$$\bar{\mathbf{q}}(t=0) = \bar{\mathbf{q}}_0 \text{ and } \dot{\bar{\mathbf{q}}}(t=0) = \dot{\bar{\mathbf{q}}}_0. \tag{5}$$

Instead of directly integrating this set of differential equations expressed in Eq. (3) subject to Eq. (5), the mode superposition method transforms it into a new set of uncoupled differential equations, simplifying the computation of the solution (Rao, 2011). Rewriting the nodal displacement vector $\bar{\mathbf{q}}$ as

$$\bar{\mathbf{q}} = \mathbf{T}\boldsymbol{\eta}, \tag{6}$$

where $\mathbf{T}$ is a transformation matrix and $\boldsymbol{\eta}$ a vector of principal coordinates, and pre-multiplying Eq. (3) by $\mathbf{T}^T$, we obtain

$$\mathbf{M}_\eta \, \ddot{\boldsymbol{\eta}} + \mathbf{K}_\eta \, \boldsymbol{\eta} = \mathbf{f}_\eta, \tag{7}$$

where $\mathbf{M}_\eta = \mathbf{T}^T \, \bar{\mathbf{M}} \, \mathbf{T}$, $\mathbf{K}_\eta = \mathbf{T}^T \, \bar{\mathbf{K}} \, \mathbf{T}$ and $\mathbf{f}_\eta = \mathbf{T}^T \, \bar{\mathbf{f}}$, subject to $\boldsymbol{\eta}(t=0) = \mathbf{T}^{-1}\bar{\mathbf{q}}_0$ and $\dot{\boldsymbol{\eta}}(t=0) = \mathbf{T}^{-1}\dot{\bar{\mathbf{q}}}_0$. A suitable candidate to form the matrix $\mathbf{T}$ is the modal basis containing the vibration mode shapes of the structure. To calculate the system's mode shapes $\boldsymbol{\phi}$ and natural frequencies ω, we define the eigenvalue problem as

$$\bar{\mathbf{K}}\boldsymbol{\phi} = \lambda \bar{\mathbf{M}} \, \boldsymbol{\phi}, \tag{8}$$

which has a solution different than zero, if, and only if

$$\det |\bar{\mathbf{K}} - \lambda \bar{\mathbf{M}}| = 0, \tag{9}$$

where $\lambda = \omega^2$ is the eigenvalue. If the matrices $\bar{\mathbf{M}}$ and $\bar{\mathbf{K}}$ are symmetrical, the eigenvectors $\boldsymbol{\phi}$ included in the modal basis $\mathbf{T}$ may be normalized in respect to $\bar{\mathbf{M}}$, such that $\mathbf{M}_\eta = \mathbf{I}$ and $\mathbf{K}_\eta = \text{diag}(\omega_i^2)$. Proportional damping can also be added to the model as $\mathbf{D}_\eta = \text{diag}(2\xi_i\omega_i)$, where ξ_i is the damping factor of mode i. Since the mass, damping, and stiffness matrices in the modal coordinates are diagonal, the equations can be uncoupled, and each one represents the influence of the individual modes in the system's response:

$$\ddot{\eta}_i + 2\xi_i\omega_i \, \dot{\eta}_i + \omega_i^2 \, \eta_i = f_{\eta_i}, \text{ for } i = 1, \ldots, \bar{n}. \tag{10}$$

However, finite element models usually have a large number of degrees of freedom $\bar{n}$ to improve the approximate solution obtained, and the cost to compute all eigenvalues and eigenvectors of a large-scale system is too high. As a result, the modal matrix $\mathbf{T}$ implemented contains only the first r eigenvectors corresponding to r smallest eigenvalues of the system, as suggested by Hatch (2000). To minimize the error created by this approximation, we chose the number of modes r, so the largest natural frequency included in the modal basis is larger than the system's sample rate. Since this still leads to a large-scale system, model order reduction methods will be applied to obtain a low-order system for the control design.

2.2 Model Order Reduction

Assuming zero initial conditions, the dynamics equation can be expressed in the state-space form as

$$\begin{bmatrix} \dot{\eta}_1 \\ \ddot{\eta}_1 \\ \dot{\eta}_2 \\ \ddot{\eta}_2 \\ \vdots \\ \dot{\eta}_r \\ \ddot{\eta}_r \end{bmatrix} = \underbrace{\begin{bmatrix} 0 & 1 & 0 & 0 & \ldots & 0 & 0 \\ -\omega_1^2 & -2\,\xi_1\omega_1 & 0 & 0 & \ldots & 0 & 0 \\ 0 & 0 & 0 & 1 & \ldots & 0 & 0 \\ 0 & 0 & -\omega_2^2 & -2\,\xi_2\omega_2 & \ldots & 0 & 0 \\ \vdots & \vdots & \vdots & \vdots & \ddots & \vdots & \vdots \\ 0 & 0 & 0 & 0 & \ldots & 0 & 1 \\ 0 & 0 & 0 & 0 & \ldots & -\omega_r^2 & -2\,\xi_r\omega_r \end{bmatrix}}_{\mathbf{A}} \underbrace{\begin{bmatrix} \eta_1 \\ \dot{\eta}_1 \\ \eta_2 \\ \dot{\eta}_2 \\ \vdots \\ \eta_r \\ \dot{\eta}_r \end{bmatrix}}_{\mathbf{x}} + \underbrace{\begin{bmatrix} \mathbf{0}_{1\times n_u} \\ \bar{\mathbf{b}}_f(1,:) \\ \mathbf{0}_{1\times n_u} \\ \bar{\mathbf{b}}_f(2,:) \\ \vdots \\ \mathbf{0}_{1\times n_u} \\ \bar{\mathbf{b}}_f(r,:) \end{bmatrix}}_{\mathbf{B}} \mathbf{u}$$

$$\mathbf{y} = \underbrace{\begin{bmatrix} \bar{\mathbf{c}}_y(:,1) & \mathbf{0}_{n_y\times 1} & \bar{\mathbf{c}}_y(:,2) & \mathbf{0}_{n_y\times 1} & \ldots \bar{\mathbf{c}}_y(:,r) & \mathbf{0}_{n_y\times 1} \end{bmatrix}}_{\mathbf{C}} \mathbf{x}, \tag{11}$$

where $\bar{\mathbf{b}}_f = \mathbf{T}^T\ \mathbf{b}_f$ and $\bar{\mathbf{c}}_y = \mathbf{c}_y\mathbf{T}$. In this representation, we can visualize the individual contribution of each mode to the system's response, from the most dominant modes with eigenvalues closer to instability to modes with eigenvalues far away from the origin, as the natural frequencies were sorted in ascending order ($\omega_1 \leq \omega_2 \leq \cdots \leq \omega_r$).

In the Modal Truncation method, we can reduce the order of this system by dividing the state vector into $\mathbf{x} = \begin{bmatrix}\mathbf{x}_1 & \mathbf{x}_2\end{bmatrix}^T$, where $\mathbf{x}_1$ contains the smallest eigenvalues, and partition the system accordingly:

$$\begin{aligned}\begin{bmatrix}\dot{\mathbf{x}}_1\\ \dot{\mathbf{x}}_2\end{bmatrix} &= \begin{bmatrix}\mathbf{A}_{11} & \mathbf{A}_{12}\\ \mathbf{A}_{21} & \mathbf{A}_{22}\end{bmatrix}\begin{bmatrix}\mathbf{x}_1\\ \mathbf{x}_2\end{bmatrix} + \begin{bmatrix}\mathbf{B}_1\\ \mathbf{B}_2\end{bmatrix}\mathbf{u}\\ \mathbf{y} &= \begin{bmatrix}\mathbf{C}_1 & \mathbf{C}_2\end{bmatrix}\begin{bmatrix}\mathbf{x}_1\\ \mathbf{x}_2\end{bmatrix}.\end{aligned} \tag{12}$$

The system's response can be approximated by simply eliminating the states $\mathbf{x}_2$, which can be assumed to contribute the least to the overall response:

$$\begin{aligned}\dot{\mathbf{x}}_1 &\approx \mathbf{A}_{11}\,\mathbf{x}_1 + \mathbf{B}_1\,\mathbf{u}\\ \mathbf{y} &\approx \mathbf{C}_1\,\mathbf{x}_1\end{aligned} \tag{13}$$

Besides sorting the system's modes according to the eigenvalues, we can sort the states based on their controllability and observability. Since those properties are not correlated, we must represent the system in a balanced realization (Laub *et al.*, 1987), where the controllability and observability grammians are equal to a diagonal matrix $\mathbf{\Sigma}$. Considering that the original system (Eq. (11)) has controllability and observability grammians $\mathbf{W}_c$ and $\mathbf{W}_o$, such balanced realization can be obtained by transforming the state vector as $\mathbf{x} = \mathbf{T}_b^{-1}\,\mathbf{x}_b$:

$$\begin{aligned}\dot{\mathbf{x}}_b &= \underbrace{\mathbf{T}_b\,\mathbf{A}\,\mathbf{T}_b^{-1}}_{\mathbf{A}_b}\mathbf{x}_b + \underbrace{\mathbf{T}_b\,\mathbf{B}}_{\mathbf{B}_b}\mathbf{u}\\ \mathbf{y} &= \underbrace{\mathbf{C}\,\mathbf{T}_b^{-1}}_{\mathbf{C}_b}\mathbf{x}_b.\end{aligned} \tag{14}$$

The grammians $\mathbf{W}_{c,b}$ and $\mathbf{W}_{o,b}$ of the balanced system are

$$\begin{aligned}\mathbf{W}_{c,b} &= \mathbf{T}_b\,\mathbf{W_c}\,\mathbf{T}_b^T\\ \mathbf{W}_{o,b} &= \mathbf{T}_b^{-T}\,\mathbf{W_o}\,\mathbf{T}_b^{-1},\end{aligned} \tag{15}$$

and the transformation matrix $\mathbf{T}_b$ is computed in such a way that

$$\mathbf{W}_{c,b} = \mathbf{W}_{o,b} = \mathbf{\Sigma} = \ \text{diag}(\sigma_i). \tag{16}$$

The diagonal elements σ_i of the balanced grammian $\mathbf{\Sigma}$ are sorted in descending order ($\sigma_1 \geq \sigma_2 \geq \cdots \geq \sigma_r$) and are called the Hankel singular values of the system. By splitting the Hankel singular values according to their magnitude, as seen in

$$\mathbf{\Sigma} = \begin{bmatrix}\mathbf{\Sigma}_1 & \mathbf{0}\\ \mathbf{0} & \mathbf{\Sigma}_2\end{bmatrix}, \tag{17}$$

with $\mathbf{\Sigma}_2 \ll \mathbf{\Sigma}_1$, we can partition the balanced representation of the system as

$$\begin{aligned}\begin{bmatrix}\dot{\mathbf{x}}_{1,b}\\ \dot{\mathbf{x}}_{2,b}\end{bmatrix} &= \begin{bmatrix}\mathbf{A}_{11,b} & \mathbf{A}_{12,b}\\ \mathbf{A}_{21,b} & \mathbf{A}_{22,b}\end{bmatrix}\begin{bmatrix}\mathbf{x}_{1,b}\\ \mathbf{x}_{2,b}\end{bmatrix} + \begin{bmatrix}\mathbf{B}_{1,b}\\ \mathbf{B}_{2,b}\end{bmatrix}\mathbf{u}\\ \mathbf{y} &= \begin{bmatrix}\mathbf{C}_{1,b} & \mathbf{C}_{2,b}\end{bmatrix}\begin{bmatrix}\mathbf{x}_{1,b}\\ \mathbf{x}_{2,b}\end{bmatrix},\end{aligned} \tag{18}$$

where $\mathbf{x}_{1,b}$ contains the most controllable and observable states. Analogously to the modal truncation discussed previously, the Balanced Truncation method eliminates the states present in $\mathbf{x}_{2,b}$:

$$\begin{aligned}\dot{\mathbf{x}}_{1,b} &\approx \mathbf{A}_{11,b}\,\mathbf{x}_{1,b} + \mathbf{B}_{1,b}\,\mathbf{u}\\ \mathbf{y} &\approx \mathbf{C}_{1,b}\,\mathbf{x}_{1,b}.\end{aligned} \tag{19}$$

Given the fact that the controllability and observability grammians can only be computed for stable systems, the balanced truncation must only be applied to the modes with eigenvalues located at the left half-side of the complex plane. The reduced system must be later augmented with the unstable states.

To analyze the performance of these model order reduction methods based on the Modal Truncation (MT) and Balanced Truncation (BT), we will compare their response in the frequency domain with the original large-scale model of the system in Eq. (11). Also, we will analyze their closed-loop performance in the time domain using an optimal controller.

2.3 Optimal Control

Consider the state-space representation of a reduced-order system:

$$\begin{aligned} \dot{\mathbf{x}}_r &= \mathbf{A}_r\, \mathbf{x}_r + \mathbf{B}_r\, \mathbf{u} \\ \mathbf{y} &= \mathbf{C}_r\, \mathbf{x}_r + \mathbf{D}_r\, \mathbf{u}. \end{aligned} \tag{20}$$

A state feedback controller can be defined as

$$\mathbf{u} = -\mathbf{K}\, \mathbf{x}_r + \mathbf{N}\, \mathbf{r}, \tag{21}$$

where $\mathbf{K}$ is the feedback gain matrix, $\mathbf{N}$ is a constant matrix, and $\mathbf{r} \in \mathbb{R}^{n_y}$ is the reference signal that the system must track as close as possible. All states in the vector $\mathbf{x}_r$ are assumed to be measurable. A linear-quadratic regulation (LQR) controller will be applied to optimize the system's response regarding state deviation and energy consumption. We want to minimize the following cost function

$$\begin{aligned} &\min_{\mathbf{u}} \int_0^\infty (\mathbf{x}_r^T\, \mathbf{Q}\, \mathbf{x}_r + \mathbf{u}^T\, \mathbf{R}\, \mathbf{u})\, dt, \\ &\text{subject to } \dot{\mathbf{x}}_r = \mathbf{A}_r\, \mathbf{x}_r + \mathbf{B}_r\, \mathbf{u}, \end{aligned} \tag{22}$$

where the diagonal matrices $\mathbf{Q}$ and $\mathbf{R}$ contain the penalty weights on the states and inputs, respectively, with $\mathbf{Q} = \mathbf{Q}^T \succeq 0$ and $\mathbf{R} = \mathbf{R}^T \succ 0$. This optimization problem can be computed by obtaining the matrix $\mathbf{S} = \mathbf{S}^T \succeq 0$ that is the solution to the continuous Riccati equation, defined as

$$\mathbf{A}_r^T\, \mathbf{S} + \mathbf{S}\, \mathbf{A}_r + \mathbf{Q} - \mathbf{S}\, \mathbf{B}_r\, \mathbf{R}^{-1}\, \mathbf{B}_r^T\, \mathbf{S} = 0, \tag{23}$$

Thus, the optimal LQR gain is

$$\mathbf{K} = \mathbf{R}^{-1}\, \mathbf{B}_r^T\, \mathbf{S}, \tag{24}$$

and matrix $\mathbf{N}$ is defined as

$$\mathbf{N} = (\mathbf{D}_r + \mathbf{C}_r\, (\mathbf{A}_r - \mathbf{B}_r\, \mathbf{K})^{-1}\, \mathbf{B}_r)^{-1}, \tag{25}$$

to guarantee that the closed-loop system has a unity DC-gain.

3. MANIPULATOR'S SETUP

As seen in Fig. 2(a), the robotic manipulator under study is the parallel and planar manipulator 3RRR with three kinematic chains containing three revolute joints. The action of three motors placed at the beginning of each kinematic chain is used to move its end-effector pose, defined by the displacements in x and y and the angular rotation α. Additionally, this manipulator has a lightweight structure designed to achieve high speeds while requiring less energy to operate. The links between the revolute joints are light as they are made of SAE 1040 steel and very thin (0.70 mm $\times$ 35 mm $\times$ 0.3 m), whereas the material of the joints and end-effector is aluminum. Using the software Comsol Multiphysics, we developed a Finite Element Model of this manipulator, as illustrated in Fig. 2(b), to simulate its dynamics in the time and frequency domains. The revolute joints of the manipulator were modeled in the multibody dynamics environment. The properties of the materials used in this model are described in Tab. 1. Tetrahedral elements were used to mesh the geometry into $\bar{n} = 23139$ degrees of freedom. Since the order of this model is too high to be used in control design, we exported the matrices $\bar{\mathbf{M}}$ and $\bar{\mathbf{K}}$ and vectors $\bar{\mathbf{f}}$ and $\bar{\mathbf{q}}$ to Matlab 2015a, which provides additional tools to perform the reduction and control strategies discussed in this paper.

Table 1. Material properties used in the 3RRR manipulator's model

Materials	Density (kg/m^3)	Poisson's ratio	Young's modulus (GPa)
Aluminum	3000	0.33	71
SAE 1040 steel	8000	0.3	200

4. RESULTS AND DISCUSSION

To represent the large-scale finite element model obtained, we considered the first 250 vibrations modes that include the natural frequencies up to 5800Hz. As discussed in the Methods section, we can sort these modes in state-space form

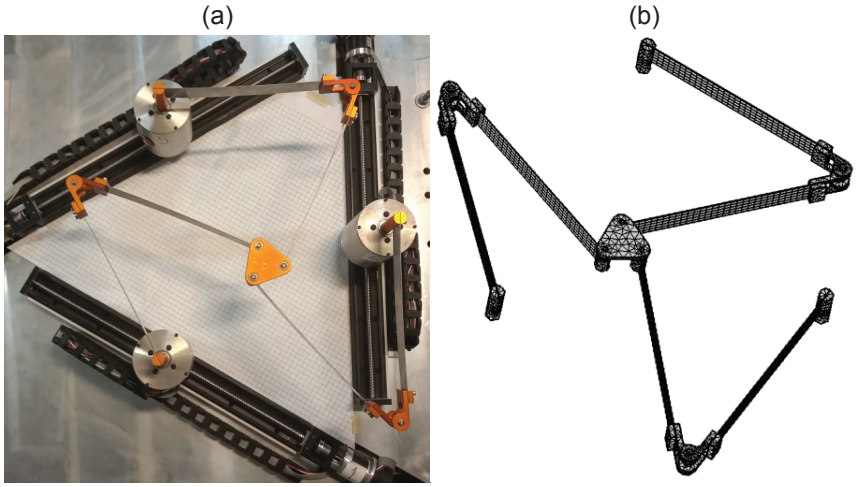

Figure 2. Parallel manipulator 3RRR under study: photo of the prototype (a) and the Finite Element model (b).

according to the natural frequencies and Hankel singular values, as seen in Fig. 3. Since the parallel manipulator has three rigid body motions, the first six states have natural frequencies of 0Hz and infinite Hankel singular values and are called unstable modes. Including natural frequencies up to twice the frequency of interest for this system, we selected to keep the first 52 states on the reduction basis of the modal truncation (up to 230Hz). For the balanced truncation, we also chose the first 52 states in the balanced realization since the energy of the eliminated states is low ($\sum_{i=53}^{500} \sigma_i / \sum_{i=7}^{500} \sigma_i = 0.0043$).

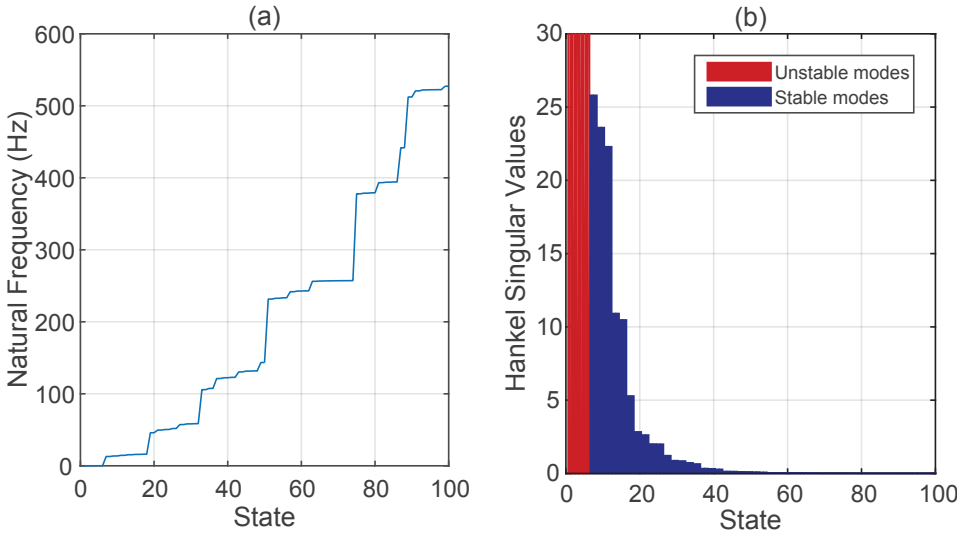

Figure 3. Sorting the states of the original model according to the natural frequencies (a) and Hankel singular values (b).

In the frequency domain, we analyzed the performance of the model order reduction methods illustrated in this paper by comparing their frequency responses with the original model, as seen in Fig. 4. The modal truncated system was able to capture all system modes up to 230Hz as defined. On the other hand, the balanced model excluded some states that are not very controllable and observable in this frequency interval and was able to capture modes up to 400Hz with the same number of states as the modal truncation system. All reduced-order systems have a good correlation with the original model's frequency response in the frequency interval of interest. Additionally, the stability of the original model, apart from the rigid-body modes, was preserved after the order reduction.

To obtain the closed-loop response of the reduced-order models, we used an optimal controller based on LQR. This numerical simulation plays an important role in the design of control strategies to be applied in the experimental setup of the parallel manipulator. We selected the state weight matrix $\mathbf{Q} = \text{diag}(100, 1, 100, 1, 100, 1, 1, \ldots, 1, 1) \in \mathbb{R}^{n_r \times n_r}$ to penalize the deviation of the three rigid-body modes more than the flexible ones, and the input weight $\mathbf{R} = \mathbf{I} \in \mathbb{R}^{n_u \times n_u}$ to apply the same penalty on all motors. For a step input in the end-effector displacement in x of 0.05m, while keeping y and α constant to zero, we investigated the closed-loop performance in the time domain of the reduced-order order models, using the modal and balanced truncation methods. As illustrated in Fig. 5, both closed-loop systems applied similar control inputs and were able to reach the steady-state response in approximately 1s. However, the transient response

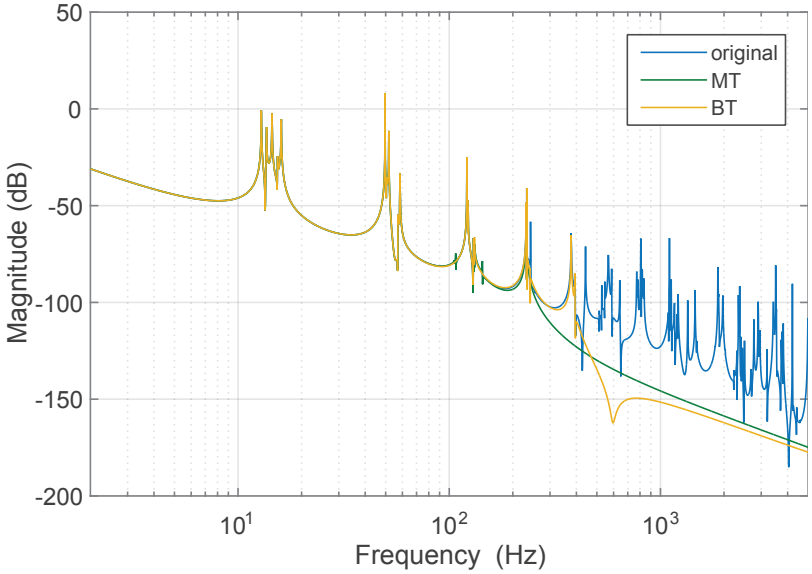

Figure 4. Frequency responses of the reduced-order models compared to the original model.

of the balanced system vibrates more than the modal truncated model, as highlighted in the displacement in y of the manipulator. To assess the cause of this increased vibration, we also evaluated the frequency response of both closed-loop systems.

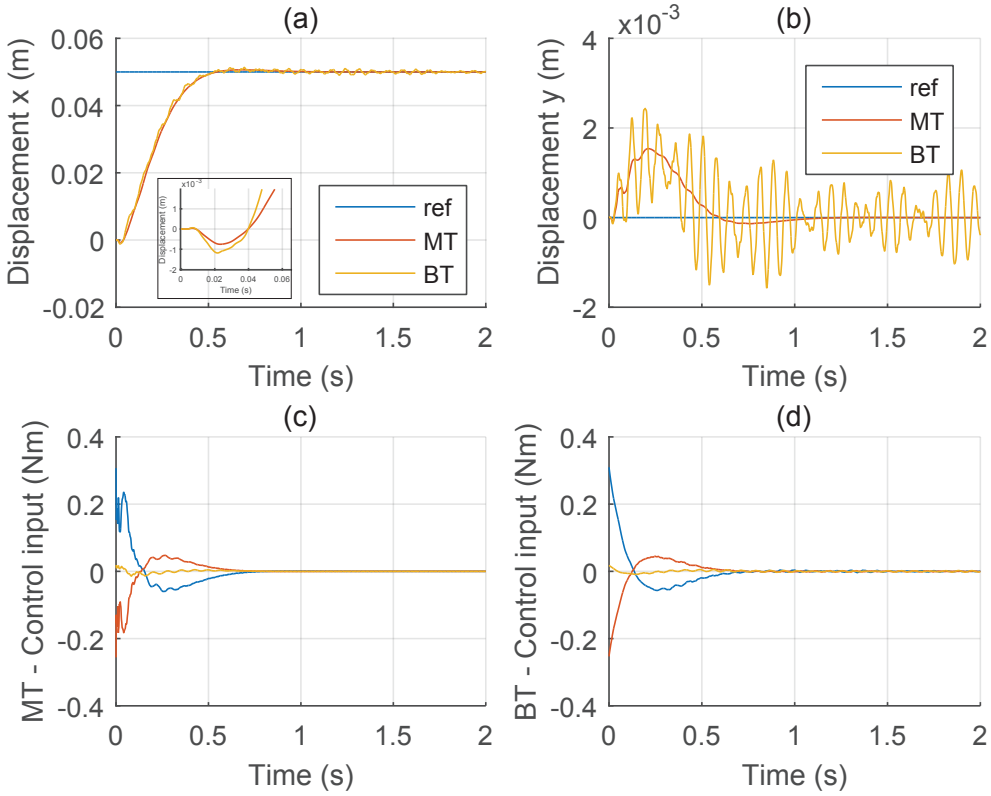

Figure 5. Displacement and control inputs of the reduced-order models in closed loop for a step trajectory.

Comparing the frequency responses of the closed-loop reduced-order models to the original model, we can note in Fig. 6 that the LQR strategy implemented was able to attenuate the resonance peaks of the modal truncated system in the frequency interval of interest. At the same time, the closed-loop control of the balanced truncated model was able to reduce only a small amount of the amplitude of the peaks. As discussed in the time response in Fig. 5, the LQR control designed is not a suitable controller to decrease the vibration of the balanced model, especially for abrupt reference trajectories such as the step function.

Alternatively, a smooth trajectory can be defined using a fifth-order polynomial with zero velocity and acceleration at

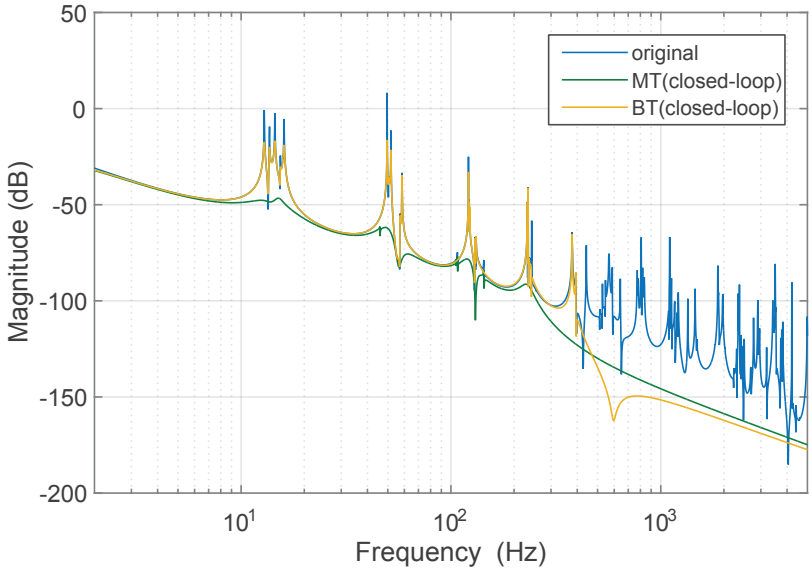

Figure 6. Frequency responses of the reduced-order models in closed-loop compared to the original model.

the beginning and end. Applying this polynomial function as a reference for the displacement in x, the time responses of the reduced-order models can be seen in Fig. 7. Although the closed-loop performance of the reduced models is satisfactory for this trajectory, both models present a delayed response. Also, the displacement in Fig. 5 first goes in the opposite direction to the reference signal as the original system has a nonminimum phase with open-loop zeros located at the right half-plane.

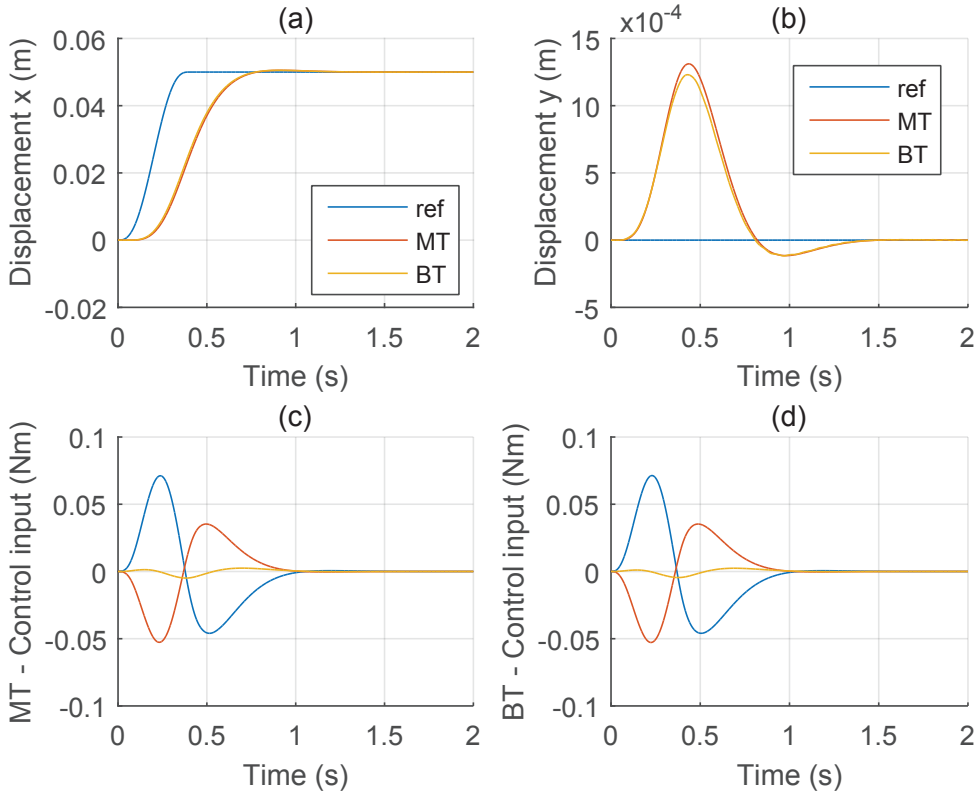

Figure 7. Displacement and control inputs of the reduced-order models in closed loop for a smooth trajectory.

Finally, Table 2 illustrates the performance of both modal and balanced truncated systems for the trajectories defined in Figs. 5 and 7. We analyzed time-domain metrics such as the root mean squared index e_{RMS} of the error between the displacement of the manipulator's end-effector and the reference signal and the energy consumption index Su, which is the sum of the absolute values of the control input $\mathbf{u}$. Both reduced-order models presented similar performance, but the balanced model presented slightly better results, notably for the polynomial trajectory.

Table 2. Performance indices of the closed-loop response of the reduced-order models using modal and balanced truncation for different trajectories.

	Fig. 5		Fig. 7	
	MT	BT	MT	BT
e^x_{RMS} (m)	0.865	0.841	0.714	0.688
e^y_{RMS} (m)	0.032	0.050	0.030	0.028
Su_1 (N m s)	0.033	0.034	0.027	0.027
Su_2 (N m s)	0.033	0.034	0.027	0.027
Su_3 (N m s)	0.033	0.034	0.027	0.027

5. CONCLUSIONS

This paper presented a model-based control strategy of a flexible parallel manipulator. We applied the finite element method to derive the manipulator's dynamics, which allows the computation of the end-effector pose and the modeling of the components' flexibility at the same time. Nonetheless, this method requires the system to be divided into tens of thousands of elements to refine the model's response. Many model order reduction methods are available in the literature, but we focused on the modal and balanced truncation. The derivation of these strategies can be done automatically and provided low-order systems. Both had a good correlation to the frequency response of the original problem and preserved the system's stability. Also, we could use the reduced-order models in the control design of the flexible manipulator, and their closed-loop responses presented a satisfactory performance in the time domain. The optimal controller was able to decrease the amplitude of the system's resonance peaks of the closed-loop frequency response, attenuating the system's vibration.

6. ACKNOWLEDGEMENTS

This research is supported by FAPESP 2018/21336-0. Fernanda T. Colombo and Maíra M. da Silva are thankful for their scholarships FAPESP 2018/22760-0 and CNPq 301338/2018-3, respectively.

7. REFERENCES

Cammarata, A. and Maddío, P.D., 2021. "A system-based reduction method for spatial deformable multibody systems using global flexible modes". *Journal of Sound and Vibration*, Vol. 504, p. 116118.

Colombo, F.T., de Carvalho Fontes, J.V. and da Silva, M.M., 2019. "A visual servoing strategy under limited frame rates for planar parallel kinematic machines". *Journal of Intelligent & Robotic Systems*, Vol. 96, No. 1, pp. 95–107. doi:10.1007/s10846-019-00982-7. URL `https://doi.org/10.1007/s10846-019-00982-7`.

da Silva, M.M., de Oliveira, L.P., Brüls, O., Michelin, M., Baradat, C., Tempier, O., Caigny, J.D., Swevers, J., Desmet, W. and Brussel, H.V., 2010. "Integrating structural and input design of a 2-DOF high-speed parallel manipulator: A flexible model-based approach". *Mechanism and Machine Theory*, Vol. 45, No. 11, pp. 1509–1519. doi:10.1016/j.mechmachtheory.2010.07.002. URL `https://doi.org/10.1016/j.mechmachtheory.2010.07.002`.

de Carvalho Fontes, J.V., Santos, J.C. and da Silva, M.M., 2018. "Numerical and experimental evaluation of the dynamic performance of kinematically redundant parallel manipulators". *Journal of the Brazilian Society of Mechanical Sciences and Engineering*, Vol. 40, No. 3. doi:10.1007/s40430-018-1072-1. URL `https://doi.org/10.1007/s40430-018-1072-1`.

Fontes, J.V. and da Silva, M.M., 2016. "On the dynamic performance of parallel kinematic manipulators with actuation and kinematic redundancies". *Mechanism and Machine Theory*, Vol. 103, pp. 148–166. doi:10.1016/j.mechmachtheory.2016.05.004. URL `https://doi.org/10.1016/j.mechmachtheory.2016.05.004`.

Géradin, M. and Rixen, D.J., 2015. *Mechanical vibrations: theory and application to structural dynamics*. John Wiley & Sons.

Hatch, M.R., 2000. *Vibration simulation using MATLAB and ANSYS*. CRC Press.

Laub, A., Heath, M., Paige, C. and Ward, R., 1987. "Computation of system balancing transformations and other applications of simultaneous diagonalization algorithms". *IEEE Transactions on Automatic Control*, Vol. 32, No. 2, pp. 115–122.

Paccot, F., Andreff, N. and Martinet, P., 2009. "A review on the dynamic control of parallel kinematic machines: Theory and experiments". *The International Journal of Robotics Research*, Vol. 28, No. 3, pp. 395 – 416.

Paccot, F., Andreff, N., Martinet, P. and Khalil, W., 2006. "Vision-based computed torque control for parallel robots". In *IECON 2006 - 32nd Annual Conference on IEEE Industrial Electronics*. IEEE. doi:10.1109/iecon.2006.347537. URL `https://doi.org/10.1109/iecon.2006.347537`.

Rao, S.S., 2011. *The Finite Element Method in Engineering*. Elsevier.

Wang, J., Wu, J., Wang, L. and You, Z., 2009. "Dynamic feed-forward control of a parallel kinematic machine". *Mechatronics*, Vol. 19, No. 3, pp. 313–324. doi:10.1016/j.mechatronics.2008.11.004. URL https://doi.org/10.1016/j.mechatronics.2008.11.004.

Yang, X., Wu, H., Li, Y., Kang, S. and Chen, B., 2018. "Computationally efficient inverse dynamics of a class of six-DOF parallel robots: Dual quaternion approach". *Journal of Intelligent & Robotic Systems*. doi:10.1007/s10846-018-0800-1. URL https://doi.org/10.1007/s10846-018-0800-1.

Yavuz, Ş. and İlman, M.M., 2020. "Modified reduced-order modeling of a flexible robot-manipulator and model-associative vibration control implementation". *Extreme Mechanics Letters*, Vol. 37, p. 100723.

Zhang, Q., Zhao, X., Liu, L. and Dai, T., 2021. "Adaptive sliding mode neural network control and flexible vibration suppression of a flexible spatial parallel robot". *Electronics*, Vol. 10, No. 2, p. 212.

Zhang, Q., Mills, J.K., Cleghorn, W.L., Jin, J. and Sun, Z., 2015. "Dynamic model and input shaping control of a flexible link parallel manipulator considering the exact boundary conditions". *Robotica*, Vol. 33, p. 1201–1230.

8. RESPONSIBILITY NOTICE

The authors are solely responsible for the printed material included in this paper.